Fuel Processing Technology 145 (2016) 76–89

Contents lists available at ScienceDirect

Fuel Processing Technology

journal homepage: www.elsevier.com/locate/fuproc

Research article

Gasification of wood particles in a co-current packed bed: Experiments and model analysis

Sadhan Mahapatra, Sandeep Kumar, S. Dasappa *

Centre for Sustainable Technologies, Indian Institute of Science, Bangalore 560012, India

ARTICLE INFO

Article history:
Received 22 October 2015
Received in revised form 19 January 2016
Accepted 26 January 2016
Available online xxxx

Keywords:
Downdraft
Gasifier
Packed bed
Propagation front
Modeling

ABSTRACT

This study focuses on addressing the propagation front movement in a co-current downdraft gasification system. A detailed single particle modeling analysis extended to the packed bed reactor is used to compare with the experimental measurement as well those available in the literature. This model for biomass gasification systems considered pyrolysis process, gas phase volatile combustion, and heterogeneous char reactions along with gas phase reactions in the packed bed. The pyrolysis kinetics has a critical influence on the gasification process. The propagation front has been shown to increase with air mass flux, attains a peak and then decreases with further increase in air mass flux and finally approaches negative propagation rate. This indicates that front is receding, or no upward movement, rather it is moving downward towards the char bed. The propagation rate correlates with mass flux as $\dot{m}''^{0.883}$ during the increasing regimes of the front movement. The study clearly identifies that bed movement is an important parameter for consideration in a co-current configuration towards establishing the effective bed movement. The study also highlights the importance of surface area to volume ratio of the particles in the packed bed and its influence on the volatile generation. Finally, the gas composition for air gasification under various air mass fluxes is compared with the experimental results.

1. Introduction

The biomass gasification process depends on a number of complex chemical reactions involving; pyrolysis, partial oxidation of pyrolysis products, gasification of the resulting char, conversion of tar and lower hydrocarbons, and gas phase reactions. Thermodynamic equilibrium and kinetic models are used to understand the complex biomass gasification process and optimizing gasifier design. Several authors have used various models to study the gasification process under various operating conditions and have carried out parametric studies with respect to equivalence ratio, gasification medium like steam, oxygen and its ratio, etc. to evaluate the influence on the output gas. Patra and Sheth have concluded that the widely used thermodynamic equilibrium model does not provide an insight into the process as equilibrium conditions are never attained in the reactor [1]. The study suggests that modeling of individual particles and packed bed including both transport and kinetic conditions is essential towards obtaining realistic predictions [1]. The study also observed that limited efforts have been directed for arriving at detailed kinetic models for downdraft gasifier; with a few contributing to address only part of the process involved in the overall gasification process like, pyrolysis, combustion, reduction zones, etc. Baruah and Baruah explored various equilibrium models for fluidized bed and downdraft gasifiers, and this study concluded that the equilibrium models has limitations due to the non-existence of equilibrium conditions inside the reactor [2]. However, modified equilibrium models with certain empirical relations based on experimental results improve its accuracy. This study also stated that the kinetic models are accurate and provide results close to the experimental results. Melgar et al. developed a mathematical model based on chemical and thermodynamic equilibrium and investigated the effect of air/fuel ratio, moisture content on the gasification performance and suggests that the reaction temperature is the driving parameter for the overall gasification process [3]. Mahmoudi et al. used eXtended Discrete Element Method (XDEM) as a framework for simulating a co-current configuration gasification system and compare the results with the experiments [4]. The experiments are conducted using diluted air (using nitrogen) and it is not evident the purpose of such dilution, except that one can infer that sub-process like pyrolysis and char gasification can be handled separately. It is also not evident based on the 25 °C air and 3% oxygen in the air, how the flaming pyrolysis process can proceed and similarly with 10% oxygen in the air in the ambient condition, enable char conversion process. The aspects related to the variation of properties like thermal conductivity, specific heat with temperature, along with the properties of the reacting fluid media have an impact; which the authors seem to have been neglected in the study. Dasappa et al. have shown that in single particle analysis, below 14% oxygen, the particle quenching (combustion ceases or reaction does not proceed) occurs at nearly ambient conditions [5]. In a separate study,

* Corresponding author.
E-mail address: dasappa@cgpl.iisc.ernet.in (S. Dasappa).

http://dx.doi.org/10.1016/j.fuproc.2016.01.032
0378-3820/

Nomenclature

$\dot{m}$	mass flow rate, kg/s
$\dot{m}_p$	gasification rate of one particle, kg/s
$\dot{m}''$	mass flux, kg/m^2 s
v_{pm}	flame front propagation velocity, mm/s
Δx	distance between two thermocouples, mm
Δt	time required to reach the reference temperature between two thermocouples, s
t	time, s
ϵ	particle porosity
ϵ_b	bed porosity
ρ	density, kg/m^3
$\overline{\rho}$	average particle density, kg/m^3
ρ_c	density of wood char, kg/m^3
Y_i	mass fraction of i^{th} species
$Y_{i,s}$	i^{th} species concentration at gas film surrounded the particle surface
T	temperature, K
T_{gas}	gas temperature, K
T_∞	ambient temperature, K
T_S	particle surface temperature, K
T_j	temperature of latitude section, K
D	diffusivity, m^2/s
D_e	effective diffusivity, m^2/s
n	number of particles per unit volume
K_D	mass transfer coefficient, kg/s
h	heat loss coefficient, W/(m^{2}K)
h_l	reactor heat loss coefficient, W/(m^{2}K)
$\dot{\omega}_i'''$	volumetric reaction rate of i^{th} specie, kg/(m^3 s)
$\dot{\omega}_c'''$	volumetric char reaction rate, kg/(m^3 s)
κ	thermal conductivity, W/(m K)
H_R	heat generation due to reaction per unit volume due to gas phase reaction, kJ/m^3
H_C	enthalpy of carbon (summation of C + CO_2, C + O_2 and C + H_2O reactions), kJ/kg
H	enthalpy of reaction, kJ/kg
C_P	specific heat, kJ/(kg K)
A_s	particle surface area, m^2
A_{sr}	surface area of the reactor, m^2
v	fluid velocity, m/s
r	particle radius, m
r_p	pore radius of wood char, m
M_g	molecular mass of the mixture of gases, kg/kmol
M_i	molecular mass of the i^{th} species, kg/kmol
V	volume of the biomass/char particle, m^3
Q	total radiative flux incident on the surface, W/m^2
τ	tortuosity factor
α	absorptivity (or emissivity) of the surface
σ	Stefan–Boltzmann constant, W/m^2 K^4
f_j	view factor
H_R''	radiative heat transfer, kJ/m^2

Subscripts

i	species CO, CO_2, H_2, H_2O and N_2
s	surface
∞	free stream

Mahmoudi et al. have addressed pyrolysis process in detail using similar modeling procedure to validate the devolatilization process [6].

Dasappa et al. modeled wood char gasification process using one-dimensional species and energy conservation equations for a single particle and extended the process to a packed char bed [5]. The process is modeled with char reacting with different reactants, diffusion and convection of species and energy in the porous medium and heterogeneous reaction between species and char. The detailed reaction mechanism for char conversion with O_2, CO_2 and H_2O are used and individually the mechanisms are validated. In the packed bed modeling, an important aspect related to flame propagation front movement against the air flow in a co-current configuration is evaluated and compared with the experimental results. It is observed that the reaction front velocity initially increases and then decreases with the increase in air mass flux and it is concluded that this happens due to the heat balance in the system. It is also found that at higher air mass flux, convective cooling of the reaction front reduces the propagation front movement. This study has been limited to charcoal as the fuel and with wood other complications like pyrolysis and the products of pyrolysis interacting within the bed poses different challenges. Sandeep and Dasappa have developed a model for packed bed biomass gasification process with dynamic variation in the evolved ambient conditions and temperature [7]. This study shows that the conversion time of the particles has a significant impact in the packed bed with varying surrounding conditions. Ranzi et al. developed a mathematical model considering pyrolysis of biomass particle, homogeneous gas phase reaction and heterogeneous reactions of the residual char at the particle level and reactor scale [8]. This study observed that residence time is an important parameter for the gasification process. Di Blasi reported a one-dimensional model for fixed bed counter-current gasifier to address the reaction front movement and gasification behavior [9]. The study analyzed in details the heat and mass transport for devolatilization, char gasification, and combustion of both char and gas species. The results arrive at the existence of a regime of decreasing temperature and propagation speed of the combustion front at near extinct conditions, attributed due to the convective cooling of the reaction front by excess air.

1.1. Propagation of flame front in packed bed

The propagation front in a packed bed can be classified as counter-current and co-current propagation relative to the direction of the air and solid fuel movement. In the case of counter-current propagation, flame front propagates in a direction opposite to that of air flow. In the case of a co-current (downdraft) configuration, apart from the flame front moving upwards into virgin fuel, the bed moves (contributed by size reduction during pyrolysis and fuel consumption) downward [10,11]. The flame front movement into the fuel bed in the upward direction against the air flow. Effective propagation rate is calculated as a sum of flame propagation rate and bed movement. Hence, the effective propagation rate has two components, the front velocity (flame propagation rate) moving into the virgin fuel bed against both the air flow and the fuel bed, and the bed movement moving downwards. In the case of, counter-current configurations, as solid fuel does not move, the effective propagation rate solely depends on the flame propagation rate.

Fig. 1 presents the schematic diagram of different reactor configurations. In the case of updraft or counter-current as well as reverse down draft configurations, air is in contact with the fuel immediately, where both the pyrolysis as well as the char combustion occurs in the reaction/combustion zone. Most of the packed bed configurations studied here is the reverse downdraft (Table 1) where the top fuel layer ignited initially, and the propagation front moves downwards into the virgin fuel bed, and the oxidiser (air) comes in contact with fuel in the combustion zone as in the case of updraft [12–16]. The front movement in reverse downdraft configuration is directly linked to the oxidiser and fuel vapor combustion zone movement. In both the above cases, there is no fuel (bed) movement which affects the propagation front. In the case of downdraft configuration, fuel, and air both moves downwards. With the flame front moving upwards into the fresh fuel, the effective or overall propagation rate is dependent on the reaction zone movement (upward) and also the bed movement (downward) due to fuel

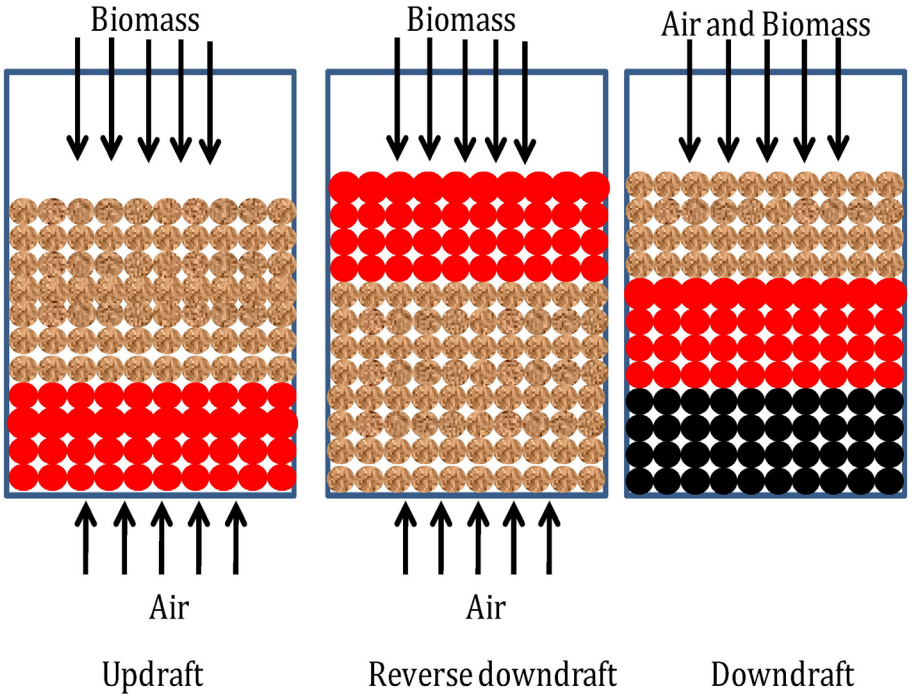

Fig. 1. Different reactor configurations.

consumption within the bed. Thus, it is important to address the effective propagation, a combination of flame front movement and the bed movement. In the case of reverse downdraft configuration, the bed movement is zero and the flame front movement, or ignition mass flux is identified as effective bed movement. In the study, of Fatehi and Kaviany, Horttanainen et al., Rönnbäck et al., Porteiro et al., and Ohlemiller et al., fixed bed reactor is used, where solid fuel does not move [12,14–17]. The air flows from the bottom (upward) where the bed is ignited and flame moves in the downward and is termed as counter-current (Porteiro et al.) [16]. However, in the present study, solid fuel moves downward along with air flow, and flame moves against the air flow and termed as co-current (reference to fuel and air flow). In the case co-current configuration (open top downdraft gasification systems), bed movement (contributed by fuel particle size reduction during pyrolysis and fuel consumption) is in the downward direction and the flame movement in the fuel bed in the upward direction against the fuel and air flow.

Most of the experiments and models reported in the literature are focused on counter-current gasification system [12–17]. Fatehi and Kavinay (1994) analyze the downward propagation of the combustion front in a packed bed of wood particles, where the air is supplied from below [12]. In this study, air flows in the opposite direction of the reaction front and the fuel bed does not move. The speed at which the burning front propagates is primarily controlled by mass flux and the initial concentrations of the oxidant. At low air mass flux, the process is limited to surface reactions and at high flow rates, both homogeneous and heterogeneous reactions take place. This study also examined the oxygen-limited and fuel-limited regimes. In the fuel-limited regime, as the air

Table 1
Fuel sample properties and reactor configurations summary.

Fuel sample	Dimension (mm)	Equivalent radius (mm)	Surface area/volume (mm^{-1})	Sphericity	Density (kg/m^3)		Void fraction	Moisture (%)	Heating value (MJ/kg)	Reactor configuration	Reference
					Bulk	Particle					
Casuarina	14 × 10 × 10	7	0.49	0.889	370	610	0.39	0	18.2	Co-current/downdraft	Present study
	14 × 10 × 10	7	0.49	0.889	370	610	0.39	10	18.2		
	17 × 13 × 10	8	0.47	0.787	345	610	0.43	5	18.2		
	20 × 12 × 10	8.5	0.47	0.773	350	610	0.43	5	18.2		
	h = 30, d = 30	17	0.20	0.874	410	610	0.33	10	18.2		
Not available	6.4	3.2	0.94	0.998	300	663	0.60	Not available	14.0	Counter-current/reverse downdraft	[12]
	10	5	0.60	0.999	200	500	0.60	10	18		[13]
Wood chips	5–20	3	1.89	0.561	157	500	0.69	10.8	Not available		[14][a]
Pine	8	4	0.75	0.999	307	579	0.47	9.1	19.3		[15]
Wood pellets	3.8	3.8	0.79	0.999	690	1180	0.42	6.2	16.3		[16]
RDF pellets	7.4	7.4	0.41	0.999	340	560	0.39	17.9	14.6		
Pine shavings	1.3	1.3	2.31	0.998	150	530	0.72	8.5	17.5		

[a] Wood chips are 5–20 mm, the average size 12.5 x 5 x 1.5 mm is considered for surface area per unit volume calculation.

flow rate increases an upper extinction limit is reached beyond which the front does not propagate through the medium. The experimental results reveal as the front moves downward, the bed height decreases due to fuel particle shrinkage. Horttanainen et al. (2000) studied the ignition front propagation against the air flow by experiment and modeling [14]. The experimental study shows that the increase of moisture of the fuel particle decreases the reaction front propagation rate, ignition front speed increases with the decrease in bed density and as the surface area/volume increase, the front propagation is faster. This study concluded that the ignited mass flow rate of the fuels per unit area of the bed (front velocity × bed density) is the important parameter while designing combustion equipment. Rönnbäck et al. (2001) investigated experimentally the influence of air flow rate and fuel samples properties on the ignition front [15]. In this study, ignition front moves opposite to the air flow. It is found from this study that as the air flow rate increases, flame propagation speed also increases and it is limited by the reaction rate of the fuel. However, at higher air flow rate, flames propagation extinct due to convective cooling of the bed. Porteiro et al. (2010) experimentally studied the ignition front in a batch type fixed bed combustor [16]. In this study, air moves upwards into the fuel bed, and solid fuel does not move. In this counter-current configuration, flame front moves downward against the air flow. This study concluded that air mass flow rate has a significant influence on ignition front propagation velocity. It is also observed that the maximum front velocity is achieved at sub-stoichiometric conditions, as the cooling effect due to excess air is minimum. Ohlemiller et al. formulated a one-dimensional model for smoldering combustion for flexible polyurethane foam assuming thermal equilibrium between gas and solid phases [17]. The configuration of the packed bed with air blown from the bottom of the bed and ignition at the top of fuel bed identified in this study as counter current configuration. This study observed that if the ignition mass flux is too low, solid will not reach a position to start the reaction and somewhat longer irradiation time is necessary to achieve the self-sustaining smolder. This study concludes that heat generation increases when the flux terminates and as the flux increases the heat generation decreases. The heat transfer process by conduction and convection dictates the smolder propagation rate, and the heat release rate and the smolder velocity are both dependent on the rate of oxygen supply (air supply rate). Very limited literature is available on the co-current gasification system, where the processes occurring in the reactor domain are very different compared to the counter-current.

Aspects related to bed parameters and influence of the input variables, such as air mass flux, fuel samples physical properties (size, density, moisture), etc. on gasification performance or producer gas composition is limited. In the present study, the model is set out for a single particle and later on extended to packed bed towards addressing the performance of a co-current packed bed reactor, and compare the model results with experimental results. The model comprises subprocess like pyrolysis, gas phase volatile combustion, and heterogeneous char reactions along with gas phase reactions in the packed bed. The following approaches are used for the analysis of thermal degradation of biomass fuel in the packed bed reactor.

(a) detailed solid and gas phase reaction mechanisms to address the variability in the thermodynamic properties in the packed bed,
(b) multi-component problem, with an approach towards variability in the biomass properties,
(c) single particle detailed analysis addressing the intra and interphase transport phenomena at the particle and the packed bed reactor and,
(d) estimation of flame front movement, bed movement, gas composition, and effects of particle size, bed temperature within the bed.

The propagation rate, gas composition and other parameters are estimated by using this model and compared with the experimental results from two different capacities/sizes gasifier using wood as a fuel and available results from the literature.

2. Methodology and experiment details

In this section, the experimental details towards evaluating the performance of a gasifier and procedure for measuring the propagation rate in packed bed are described. Fig. 2 represents a reactor with the K-type thermocouple arrangement. This reactor is insulated with ceramic wool throughout the length to reduce the heat losses from the outer wall of the reactor. An air nozzle is provided on one side of the reactor for ignition purpose as shown in Fig. 2. This air nozzle is 620 mm below the gasifier top. All the experiments are performed in sub-stoichiometric or gasification regimes only. Casuarina (*Casuarina equisetifolia*) wood is used as fuel in the gasifier. The specifications of the reactor, biomass particle size, moisture contents and types of reactor configurations are used in the experiments and the reported data from the literature are presented in Table 1. All the available reactor configurations used in this study from the literature are counter-current where solid fuel does not move; air flow in upward and flame movement is in the downward direction [12–16]. However, the reactor configuration used in the present study is co-current, where solid fuel and air moves downward and flame propagates in the upward direction. Table 2 presents the ultimate and proximate analysis of the biomass sample used in the experiments. Initially, the reactor is loaded with charcoal up to the ignition port and for the rest of its height is filled with wood samples of a particular size. A blower is used to provide the required suction to draw the air through the top and the nozzle. After ignition, the air nozzle is closed, allowing all the air to be drawn from the top for the gasification process. During this period, the temperature at various locations of the reactor

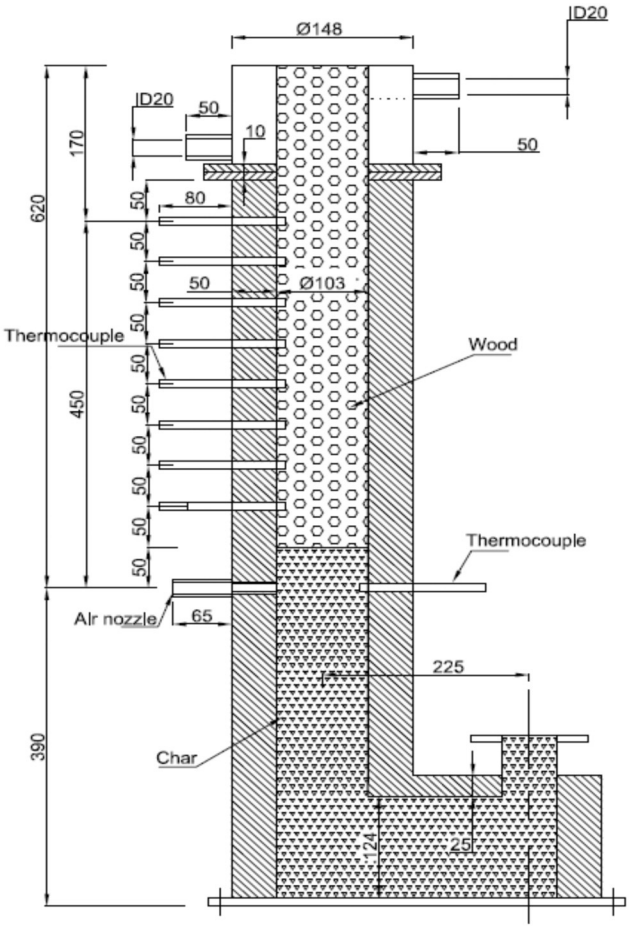

Fig. 2. Thermocouple arrangement in the reactor (103 mm diameter).

Table 2
Biomass sample properties.

Parameter	Ultimate analysis (% dry basis)	Parameter	Proximate analysis (% dry basis)
C	42.830	Fixed carbon	18.38
H	6.236	Volatile matter	81.28
N	0.124	Ash content	0.34
S	0.419	Calorific value (MJ/kg)	18.2
O[$]	50.391	[$] Measured by difference of weight	

and the gas composition are recorded. The biomass feeding rate is measured by measuring the average biomass feed per hour into the reactor during its operation. The bed movement is arrived at by actually measuring the bed movement (downward) per unit time interval and is verified based on the fuel consumption. The flame propagation movement (v_{pm}) is determined by the following relation.

$$v_{pm} = \frac{\Delta x}{\Delta t}$$

where Δx is the distance between two thermocouples and Δt is the time required to reach the reference temperature 500 °C between these two thermocouples. The time required to reach the reference temperature is calculated by using the temperature profile. The detailed experimental set up is presented in Mahapatra and Dasappa [10]. Experiments are conducted to calculate the propagation rates in packed bed under different air mass flux. The propagation rate in packed bed of wood particles is measured in two reactors of 103 mm and 350 mm diameters with different fuel size. Effective propagation rate is calculated as a sum of flame propagation rate and bed movement.

3. Modeling of particles in packed bed

In the co-current configuration, biomass moves from the top of the reactor along with the air and the output gases are drawn from the bottom of the reactor. Biomass consumption and gas flow rates depend on the air mass flux. Hence, any changes in the gas flow rate resulted in the changes in the bed movement (due to biomass consumption and shrinkage). The biomass particle inside the reactor is exposed to varying reaction environment from the reactor top on its way to the bottom ash pit. The physical processes occur for single particle are modeled by using unsteady spherically symmetric one-dimensional conservation equations. The assumptions made in this model are (i) conversion process is in one-dimensional, (ii) pressure gradient within the particle is neglected since the porosity of the particle is high, (iii) uniformity in temperature between gas and solid (char), (iv) uniformity in the emissivity of entire of the biomass/char particle and (v) volatile constitutes 80% of the particle weight and rest 20% is char or fixed carbon (typical for woody biomass). The gasification process is like a transition from solid biomass to gaseous phase due to the reaction inside the particles. As the solid biomass converted (due to reaction) to gases, the porosity of the solid (char) particles also changes (increasing). The assumption for packed bed analysis are (i) gasifier reactor is considered as control volume with individual particles as a point source in the bed with a given bed porosity, (ii) quasi-steady conditions in the continuity equation neglecting the time derivative term and (iii) model analysis is carried out by setting out the conservation equations for mass, species, and energy. Properties of bulk fluid vary continuously as the reaction proceeds. These are determined by solving the set of conservation equations assuming variations only across the bed height.

Fig. 3 presents a schematic diagram of the process occurring in the packed bed. The single-particle model involving pyrolysis and detailed reaction kinetics for char gasification is extended for the modeling of the packed bed of biomass particles. The philosophy used in the model is similar to the one used by Dasappa and Paul for packed bed of char where the packed bed is divided into a number of layers, or computational cells, and conservation equations for a typical particle representing each cell are solved [11]. The mass conservation equation in rectangular coordinates is;

$$\frac{\partial(\rho\varepsilon)}{\partial t} = -\nabla.(\rho V) + \dot{\varpi}_c'''. \tag{1}$$

Neglecting the time derivative term in Eq. (1) (assuming quasi-steady conditions in the continuity equation) the above equation in x-direction (along the bed height) translates to;

$$\frac{\partial(\rho u)}{\partial x} = \dot{\varpi}_c'''. \tag{2}$$

The superficial mass flux passing through the bed is $\dot{m}'' = \rho u$, and the volumetric char reaction rate term ($\dot{\varpi}_C'''$) can be substitute with $n\dot{m}_p$. Here, u is the superficial velocity of gas, n is the number of particles per unit volume, $\dot{m}_p$ is the gasification rate which signifies the conversion rate and derived from the solution of single particle analysis. Hence, Eq. (2) can be written as;

$$\frac{\partial(\dot{m}'')}{\partial x} = n\dot{m}_p. \tag{3}$$

Heat transfer between the particle and the surrounding particles, and properties of the bulk fluid surrounding the particles is used in the packed bed analysis apart from single particle considerations. These are determined by solving a set of conservation equations for the bulk gases assuming variations only with the height of the bed (x-direction). The species conservation equation is as follows

$$\frac{\partial(\rho\epsilon_b Y_i)}{\partial t} + \frac{\partial(\dot{m}'' Y_i)}{\partial x} = \frac{\partial}{\partial x} D\rho \frac{\partial Y_i}{\partial x} + n[\dot{m}_p Y_{i,s} + K_D(Y_{i,s} - Y_i)] + \dot{\varpi}_i'''. \tag{4}$$

Here, K_D (kg/s) is the mass transfer coefficient through the gas film surrounding the particle. The second term on the right-hand side of Eq. (4) represents the mass production of species Y_i in the packed bed. The third term on the right hand side represents the product of number of particles per unit volume (n), mass transfer from the concentration $Y_{i,s}$ to Y_i. The bed porosity (ϵ_b) is considered in place of char porosity (ϵ). The gas phase energy conservation equation is represented by Eq. (5).

$$\frac{\partial(\rho\epsilon_b C_P T)}{\partial t} + \frac{\partial(\dot{m}'' C_P T)}{\partial x} = \frac{\partial}{\partial x}\kappa\frac{\partial T}{\partial x} + H_R + n[\dot{m}_p C_P T_{gas} + hA_s(T_{gas} - T)] + h_l A_{sr}\Delta T \tag{5}$$

The first term of the right-hand side of Eq. (5) represents the effective conductive heat transfer to a single particle in the control volume, the second term represents the heat generation due to reaction per unit volume due to gas phase reaction, the third term represents the heat carried away by the hot gases, the fourth term represents the convective heat that transfer from the gas films to surroundings and the last term is the heat loss from the reactor wall. Radiation is the major mode of heat exchange, and conduction has very little effect, as the contact between the particles in a packed bed is very small and emissivity of the char particle is high [18]. A particle views the surrounding particles at various heights with different temperature. It has been considered that all particles have a uniform surface temperature representing the average height at which these particles reside within the bed, and the emissivity of all the particles are also same. The total radiative flux falling on the sphere and the net radiation absorbed is estimated by using the following equations [18]

$$Q = \sum_j f_j \sigma T_j^4 \tag{6}$$

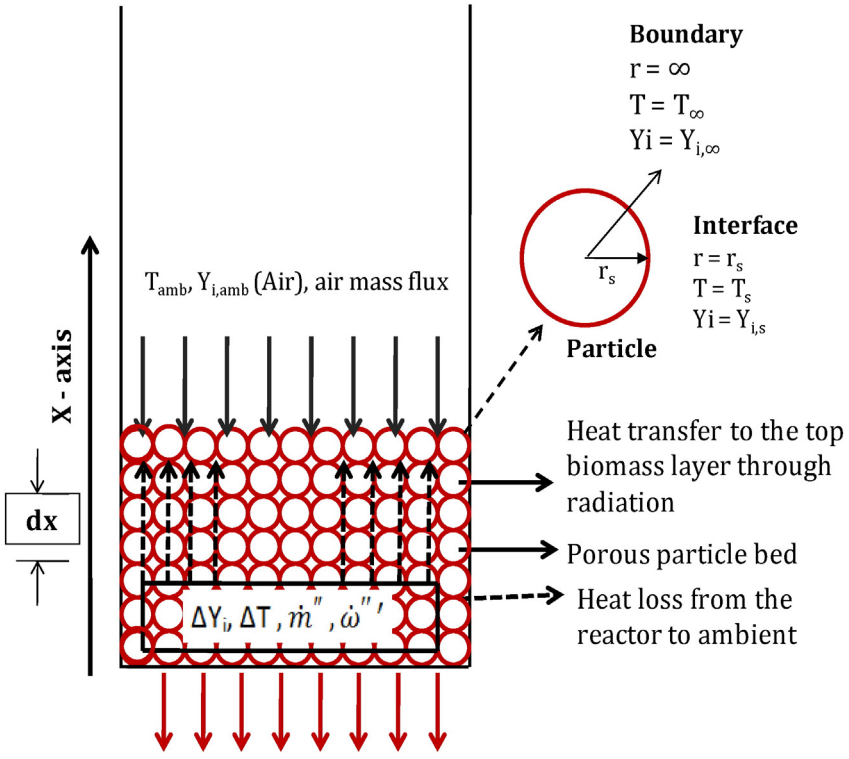

Fig. 3. Packed bed representation for analysis.

$$H_R'' = A_s\alpha\left(Q - \sigma T_s^4\right) \tag{7}$$

where Q is the total radiative flux incident on the surface, A_s is the surface area of the sphere and α is the absorptivity (or emissivity) of the surface.

3.1. The governing equations for single particle

The physical processes that occur for a single particle are modeled by using unsteady spherically symmetric one-dimensional conservation equations. With the conversion of solid biomass to gaseous phases and char, the porosity of the solid (char) particles changes (increasing) and this is used to estimate the end of conversion (porosity becomes one). The governing mass, energy and species conservation equations are

$$\frac{\partial}{\partial t}(\rho\epsilon) = \frac{1}{r^2}\frac{\partial}{\partial r}(-\rho v r^2) + \dot{\varpi}_c''' \tag{8}$$

$$\frac{\partial}{\partial t}(\rho\epsilon Y_i) = \frac{1}{r^2}\frac{\partial}{\partial r}\left(-\rho v r^2 Y_i + r^2\rho D_e\frac{\partial Y_i}{\partial r}\right) + \dot{\varpi}_i''' \tag{9}$$

$$\frac{\partial}{\partial t}(\rho C_P T) = \frac{1}{r^2}\frac{\partial}{\partial r}\left(-\rho v r^2 C_P T + r^2\kappa\frac{\partial T}{\partial r}\right) - H_c\dot{\varpi}_c''' \tag{10}$$

$$\frac{\partial\epsilon}{\partial t} = -\frac{\dot{\varpi}_c'''}{\rho_c}. \tag{11}$$

3.2. Initial, interface and boundary conditions and solution methods

The conservation equation (Eqs. 8–11) presented in the earlier section is solved by using initial, interface and boundary conditions. The initial conditions at $t = 0$ (time) are the temperature and concentration profiles within the particle. The temperature is set to the ambient condition or the condition dependant on the experimental requirement. The precise nature is not very important as the transient condition dies down in a small fraction of the conversion time. This is due to diffusion dependant heterogeneous reactions. The boundary conditions are at large distance from the particle ($r \to \infty$), the temperature is set to be $T \to T_\infty$ and at the particle surface ($r = r_S$), temperature is considered to be $T = T_S$.The unsteady spherically symmetric one-dimensional energy and species conservation equations in case of quasi-steady gas phase are as follows

$$\frac{\dot{m}C_P}{4\pi r^2}\frac{\partial T}{\partial r} = \frac{1}{r^2}\frac{\partial}{\partial r}\left(r^2\kappa\frac{\partial T}{\partial r}\right) \tag{12}$$

$$\frac{\dot{m}}{4\pi r^2}\frac{\partial Y_i}{\partial r} = \frac{1}{r^2}\frac{\partial}{\partial r}\left(r^2 D_e\rho\frac{\partial Y_i}{\partial r}\right). \tag{13}$$

The solution of Eqs. (12) and (13) is evaluated assuming Lewis number to be in unity. The solution of energy and species energy conservation equations is rewritten in the following form

$$\frac{(T - T_\infty)}{(T_S - T_\infty)} = \frac{(Y_i - Y_{i\infty})}{(Y_{is} - Y_{i\infty})} = \frac{(1 - \eta)}{(1 - \eta_S)} \tag{14}$$

where $\eta_S = \exp(-\frac{\dot{m}C_P}{4\pi\kappa r_S})$ and $\eta = \exp(-\frac{\dot{m}C_P}{4\pi\kappa r})$.

The subscript 's' refers to the value at the surface of the sphere. Differentiating Eq. (14), at the surface $r = r_S$ provides the interface conditions both for energy and species conservation equations and final form of the equations are as follows.

$$\kappa\frac{\partial T}{\partial r} = C_P Q(T_\infty - T_S) - \dot{R}'' \tag{15}$$

$$D\rho\frac{\partial Y_i}{\partial r} = Q(Y_{i\infty} - Y_{iS}) \tag{16}$$

where $Q = \left[\frac{\dot{m}}{4\pi r_s^2}\frac{exp(-B_0)}{\{1-\exp(-B_0)\}}\right]$, $B_0 = \frac{\dot{m}C_P}{4\pi\kappa r_s}$ *and* $\dot{R}''$ is the radiative heat flux from the surface of the sphere.

The energy and species conservation equations are integrated and same initial, and boundary conditions stated earlier are used for its solution. The independent variable '*r*' is transformed into the volume *(V)* to make the equations fully conservative and remove the singularity at r = 0. The transformed energy and species conservation equations are as follows

$$\frac{\partial}{\partial t}(\overline{\rho}C_P T) = \frac{\partial}{\partial V}\left(-\dot{m}C_P T + (4\pi)^{2/3}(3V)^{4/3}\frac{\partial T}{\partial V}\right) - H_C\dot{\varpi}_C''' \tag{17}$$

$$\frac{\partial}{\partial t}(\rho Y_i \epsilon) = \frac{\partial}{\partial V}\left(-\dot{m}Y_i + D_e\rho(4\pi)^{2/3}(3V)^{4/3}\frac{\partial Y_i}{\partial V}\right) + \dot{\varpi}_i''' \tag{18}$$

where $\dot{m} = \rho A v_S = 4\pi r^2 \rho v_S$. The mass flow rate of the gases comes out from the porous char and to be consistent with respect to the unsteady formulation, the equation of state is used to get the following relation.

$$\frac{\rho\epsilon}{\overline{\rho}}\frac{\partial(\rho\epsilon)}{\partial t} + \rho\left(1 - \frac{\rho_C\epsilon}{\overline{\rho}}\right)\frac{\partial\varepsilon}{\partial t} - M_g\sum\frac{1}{M_i}\frac{\partial}{\partial t}(\rho\varepsilon Y_i) - \left(\frac{\rho\epsilon}{\overline{\rho}TC_P}\right)\frac{\partial}{\partial t}(\overline{\rho}C_P T) = 0. \tag{19}$$

3.3. Kinetics of the reaction mechanisms and choice of parameters

Pyrolysis as a process or thermal decomposition of wood releases volatiles leaving behind the carbon in the form of porous char. The lower temperature regime of decomposition of wood showed that mainly H_2O, CO_2 and CO are evolved and at the higher temperature regime, the primary decomposition products are oil, H_2O, H_2, hydrocarbon gases and lower concentrations of CO and CO_2. The particles are subjected to varying temperature profiles as they travel through the packed bed, also allowing for the possibility of combustion of some of the volatiles. Based on the particle size and the heat flux, predominantly slow pyrolysis takes place in case of the gasification process. Typically for the reactor configuration considered in the study, slow pyrolysis prevails with very low heating rates (less than 5 K/s), and char is the primary output along with gases. While addressing the overall packed bed model, conservation of enthalpy and the elemental balance of C, H and O are more relevant for pyrolysis than characterization of the species in the volatiles and kinetics of volatile cracking or combustion. The output products of volatiles in the gasification process are primarily CO and H_2, with a little amount of CH_4 [7]. The pyrolysis reaction is assumed to be slightly endothermic with the heat of reaction being −0.42 MJ/kg [9]. Further, these gases undergo stoichiometric combustion and release heat of reaction. The following reaction takes places in this process.

$$CH_{1.4}O_{0.6}\ (\text{wood}) \rightarrow C_{0.616}H_{1.4}O_{0.6}(\text{volatiles}) + 0.384\ C\ (\text{char}) - 0.42\ \text{MJ/kg}$$

$$C_{0.616}H_{1.4}O_{0.6}\ (\text{volatiles}) + 0.008\ O_2 \rightarrow 0.016CH_4 + 0.6CO + 0.668H_2 + 59.8\ \text{MJ/kg}$$

$$CO + \frac{1}{2}O_2 \rightarrow CO_2 + 10.08\ \text{MJ/kg}$$

$$H_2 + \frac{1}{2}O_2 \rightarrow H_2O + 141.65\ \text{MJ/kg}$$

$$CH_4 + 2O_2 \rightarrow CO_2 + 2H_2O + 55.52\frac{\text{MJ}}{\text{kg}}.$$

The following three important overall reactions are considered in the analysis with respect to char combustion. The reaction rate and various constants used in the model along with the references are presented in Table 3.

$$C + O_2 \rightarrow CO_2$$

$$C + CO_2 \rightarrow 2CO$$

$$C + H_2O \rightarrow CO + H_2.$$

The physical, thermodynamic and transport properties used in the model are taken from literature. The density of non-porous char particle (ρ_c) and the calorific value (H_c) of carbon are taken from Dasappa [18]. The pore radius (r_p), tortuosity factor (τ) are chosen from Groeneveld [19]. The non-porous char (k_c) and gas (k_g) thermal conductivity are chosen from Dasappa [18] and the porous char conductivity is 0.4–0.5 [20]. The thermal conductivity of gas phase (k_g) is calculated taking into account the presence of H_2. The un-reacted char porosity is chosen from Dasappa [18]. The various parameters used in the model are presented below.

$$\rho_c = 1900\ \text{kg/m}^3, \rho_b = 610\ \text{kg/m}^3, r_p(t=0) = 50\ \mu\text{m}, C_p = 1.25\text{KJ/kg}$$

$$H_c = 32.6\text{MJ/kg}, k_c = 1.85\text{W/mK}, k_g = 0.071\ \text{W/mK}, \tau = 1.5$$

$$\varepsilon = 0.88\ (\text{unreacted char}).$$

3.4. Solution procedure

The packed bed is divided into a number of computational cells with height *dx* (Fig. 3). The conservation equations of a single typical particle representing each cell are solved. The single particle is solved and its output, in terms of gas species and energy released or diffused translates to being a source term for the packed bed. At initial fractional time step, the conservation equations for the sphere are solved. One representative sphere is solved in each computational cell along the height of the bed. Solutions of the equations of the particle provide the conditions at the surface of the sphere, and the net mass flux from the sphere is used in the next fractional time step when Eqs. (8–11) are solved. These equations are solved to obtain the variation of properties in the gas phase. Knowing the temperature profile, at a particular location in a given cell, the temperature at other locations is obtained through interpolation. Thus, the temperature distribution within the bed is obtained. In this study, the model is used to obtain the temperature profile, gas composition at different time interval. The input parameters are particle diameter and air mass flux. The model provides output temperature profile for a particular air mass flux, and this is used to calculate the propagation rate in that particular air mass fluxes. The detailed results and its analysis comparison with experimental results are presented in the following sections.

4. Results and discussion

The following section summarizes the results from the model and compares with those from the present experimental study and also from the literature. Aspects related to the bed temperature, gas composition, and propagation rate, which depict the overall performance of the packed bed reactor, is used for comparison. Validation of the model for pyrolysis has been extensively carried by Sandeep and Dasappa for both inert and reactive environment and also extended the analysis to packed bed [7].

4.1. Temperature profile in the packed bed

Fig. 4 represents the typical temperature profile obtained from the model at an air mass flux of 0.105 kg/m^2/s. Flame propagation rate

Table 3
Rate expression used in the model.

Reaction	Rate expression	Constant	Reference
$C + O_2$	$\varpi''_{C+O_2} = -\frac{M_c S_1 S_2 X_{os}}{(S_1 X_{os}+S_2)}$ $S_1 = A_c P\, exp(-\frac{E_1}{RT})/(\sqrt{2\pi M_{O_2} RT})$ $S_2 = A_f\, exp(-\frac{E_2}{RT})$ $\varpi'''_{C+O_2} = \frac{2\varpi''_{C+O_2}\varepsilon}{r_p}$	A_c: 1/150 E_1/R: 1700 K E_2/R: 20,000 K A_f: 0.0875 mol/m^2-s	[18,21]
$C + H_2O$	$\varpi'''_{C+H_2O} = -\frac{k_1 p_{H_2O}+K_4 p_{H_2} p_{H_2O}+K_5 p^2_{H_2O}}{1+K_2 p_{H_2}+K_3 p_{H_2O}}$	$k_1 = 3.6\times10^7$ mol/cm^3-s-atm $K_2 = 35$ atm^{-1}, $K_3 = 0.025\times10^{-6}$ atm^{-1} $K_4 = 2.1\times10^{-3}\exp(E_4/RT)$ atm^{-1} $K_5 = 91.8\exp(E_5/RT)$atm^{-1}	[11,22]
$C + CO_2$	$\varpi'''_{C+CO_2} = -\frac{k_1 p_{CO_2}-K_2 p^2_{CO}}{1+K_3 p_{CO}+K_4 p_{CO_2}}$	$k_1 = 2.2\times10^9\exp(E/RT)$mol/cm^3-s-atm $K_3 = 15.0$ atm^{-1}, $K_4 = 0.25$ atm^{-1} $K_2$is obtained from equilibrium	[18]
$CO + H_2O$	$K_p = \frac{p_{CO2}\, p_{H2}}{p_{CO} p_{H2O}}$ $K_p = exp^{(\frac{a_1}{T}+a_2+T(a_3+T(a_4+T(a_5+T\times a_6))))}$	$a_1 = 4.89\times10^3$, $a_2 = 4.75$, $a_3 = 1.28\times10^{-3}$, $a_4 = 2.89\times10^{-6}$, $a_5 = 1.76\times10^{-9}$ and $a_6 = 3.77\times10^{-13}$	[23]
Pyrolysis	$\omega'''_{pyr} = A_{pyr}\, X_{bio}\exp(-\frac{E_{pyr}}{RT})$	$A_{pyr} = 1.44\times10^4$ s^{-1} $E_{pyr} = 88.6$ KJ/mol X_{bio} is the biomass fraction available at a given time	[7,9]

(Fig. 4) in the model is calculated as the difference between effective propagation rate and bed movement. The bed movement is evaluated considering the shrinkage of particles (during pyrolysis) and carbon conversion (during char reduction). Shrinkage of the particle diameter is typical about 10% as detailed measurements carried in the laboratory, and the reduction in the char diameter is estimated based on the layers of carbon conversion occurring due to the chemical reactions at the surface depending upon the reacting species in the vicinity of the particle undergoing the conversion. This temperature profile (Fig. 4) is similar to the profile obtained from the experiment (Fig. 5). After the ignition, the air nozzle is closed in the experiments and model also follows similar by drawing the air from the top of the reactor. It is observed that the propagation front is moving from the ignition point towards the top of the reactor. The propagation rate as predicted from the model at an air mass flux of 0.105 kg/m^2/s is 0.081 mm/s (Fig. 4) and from experiment, it is 0.083 mm/s at an air mass flux of 0.12 kg/m^2/s (Fig. 5). These results show a reasonable match between the model and experimental results despite small differences in the peak temperatures recorded. This small difference is justified based on the estimation of heat loss from the reactor based on the choice of the heat transfer correlations. Groeneveld and Mukunda et al. have estimated that 8–10% of the input energy is lost in a typically insulated gasifier [19,24]. Dasappa estimated that the difference in peak temperature in the case of heat loss and without heat loss consideration, from the reactor, is about 170 K for a charcoal gasifier experiment [18]. In this model, heat transfer coefficient of 10 W/m^2-K is considered in the calculation based on the results from Dasappa and Paul [11].

4.2. Propagation rate and peak temperature in the bed

It is observed from Fig. 6 that flame front movement or propagation rate increases as the air mass flux increases, attains a peak and any further increase in air mass flux, the propagation rate decreases. The model predicts the peak propagation rate as 0.094 mm/s at an air mass flux of 0.135 kg/m^2/s; while it is 0.089 mm/s at an air mass flux 0.132 kg/m^2/s from the experimental results. The similar trend of flame front propagation is also observed by Dasappa and Paul for the co-current gasifier using charcoal as the fuel, except that the peak propagation rate for charcoal was 0.30 mm/s [11]. The difference between these values is related with the properties of the fuel with wood having 80% volatiles while charcoal has less than 10% volatiles [25].

Fig. 6 also presents the model predictions and experimental results for the peak temperature in the bed at different air mass flux and is found to follow a similar trend. It is found that the model estimated temperature, on average 85 K higher than the experimental measurement. This is attributed to the choice of heat transfer coefficient for the model based on the earlier works [11]. It is evident from the analysis that the experimental reactor effective insulation is different, and hence the heat loss is comparatively higher. However, by increasing the heat transfer coefficient in the model to 14 W/m^2-K, predictions are found

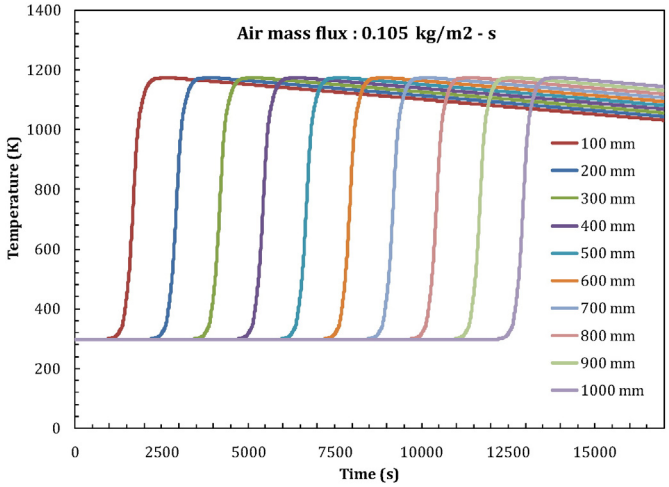

Fig. 4. Temperature profile from model inside the reactor.

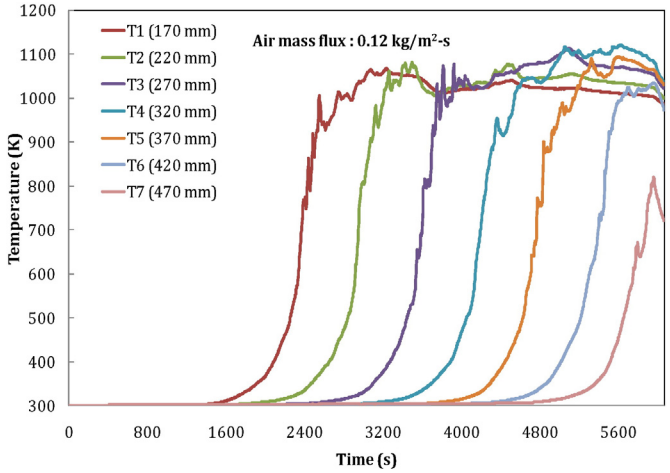

Fig. 5. Temperature profile from experiment inside the reactor.

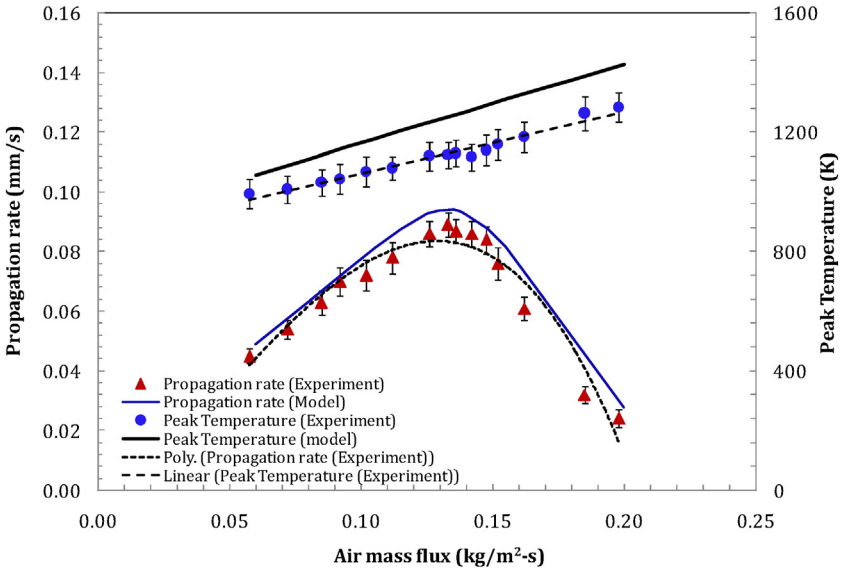

Fig. 6. Propagation rate and bed peak temperature at various air mass flux.

to be closer to the present experiments. It is found from Fig. 7 that during the increasing profile of the propagation rate regime, the propagation rate correlates with mass flux as $\dot{m}''^{0.883}$ which is different compared to the work on charcoal ($\dot{m}''^{0.36}$) [11]. In this present study, wood is used as fuel and major part of the fuel is consumed while the reaction front passes through the bed. In the case of charcoal, only a small fraction of the fuel is consumed in the reaction front. In both the cases, it is under fuel rich conditions unlike other studies [12–16]. The reaction front heats up more fuel in the case of charcoal than it consumes and this has influence on both the peak temperature and the propagation rate. It has been argued that rate of increase of front velocity with air mass flux is less than the rate of increase of mass flux itself, the peak temperature at the front increases with air mass flux also aided by the increased heat and mass transfer coefficients between the particle and gas [11]. Further, it is also important to highlight that the specific heat of biomass and endothermicity in the pyrolysis process of biomass and density difference between these two fuels leads to lower propagation rate for wood compared to charcoal. It is also observed from the experiments and model analysis, that further increase of the air mass flux resulted in reduction in the absolute value of propagation rate leading to extinction.

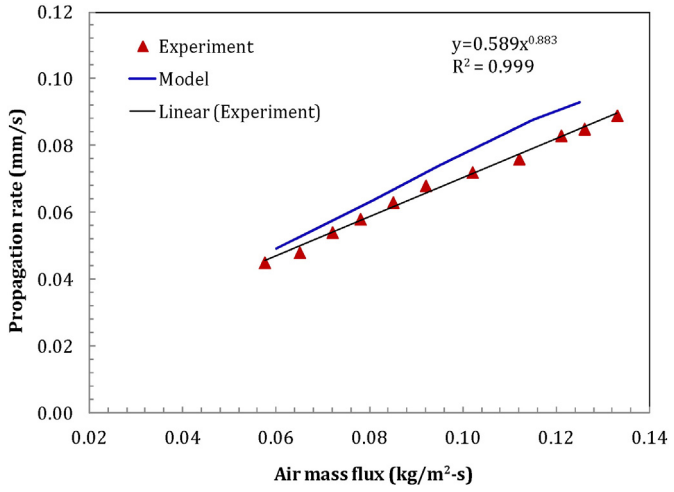

Fig. 7. Propagation rate variation with air mass flux at the increasing regime of propagation rate.

It is important to highlight, that the flame front movement in a packed bed, in general, depends on factors involved in the fuel consumption rate, energy balance and heat generation by chemical reaction, heat loss through radiation, heat transfer to unburnt fuels, convective cooling due to the air flow along with the heat loss from the reactor surface. At lower air mass flux, pyrolysis rate being lower, the energy release through volatile combustion is lower, resulting in lower bed temperature. With the increase in air mass flux, ensuring higher oxidiser environment improves the heat generation process resulting in higher bed temperature. This in turn improves the pyrolysis rates and also leads to higher propagation front movement. The possible reasons for the peak propagation front movement attaining the peak, along with an increase in temperature is addressed by considering the balance between heat generation and heat loss. Any further increase in the air mass flux, heat loss component dominates, and thus the propagation rate tends to decrease [10–12,15], which provides justification for such behavior.

Fig. 8 presents the model prediction of propagation front, for two different air mass fluxes and for two different time intervals. With an air mass flux of 0.105 kg/m^2/s, the front movement is upwards into the fuel bed countering the air flow, while in the case of air mass flux at 0.235 kg/m^2/s, it shows that the front moves in the reverse direction, along with air flow. This behavior suggests that the flame front is receding even though the bed temperature is higher. This phenomenon also indicates that beyond this air mass flux (0.235 kg/m^2/s), the reactor ceases to function as an open top gasifier reactor but approaches towards closed top configuration, where most of the process occur below the air injection port/nozzle.

In case of co-current reactor, both the fuel and the reactant move in the downward direction (Fig. 1). It can be observed from Fig. 9 that with the increase in air mass flux, the propagation front attains a peak and then reduces; bed movement increases linearly with the increase in air mass flux due to biomass consumption and shrinkage of particle due to pyrolysis as well as char conversion. Therefore, the effective propagation movement which is summation of flame front and bed movement also increases gradually with the increase in air mass flux till it reaches the extinction limit.

Table 4 presents the flame propagation rate, bed movement and effective propagation at various air mass fluxes from the experimental results. The flame propagation and bed movements are measured during the experiment. It can be observed that with the increase in air mass flux, the flame propagation increases and later reduces, but the bed movement gradually increases (Fig. 9). Towards analyzing the aspects

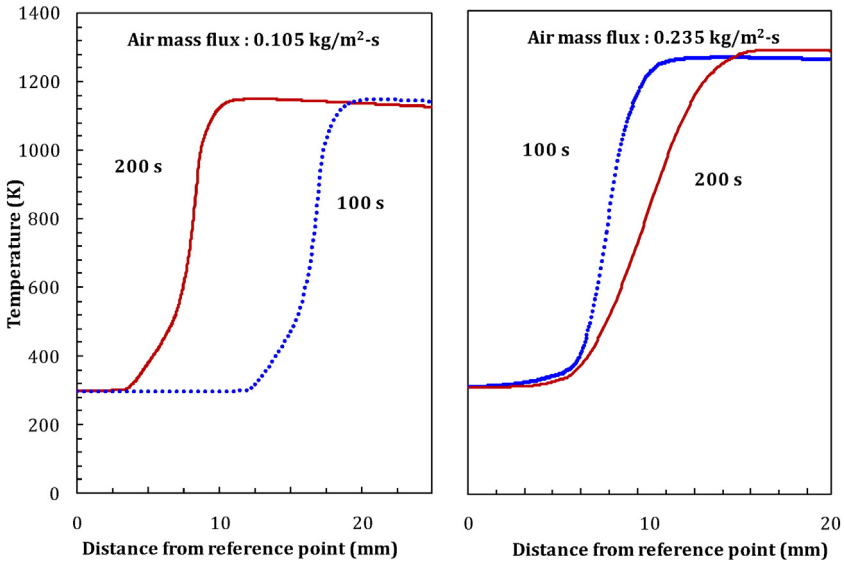

Fig. 8. Temperature profiles at two different air mass flux.

related to the effective propagation rate, experimental data related to bed movement and propagation rate are used and compared with the estimated bed movement using bed properties. The biomass consumption at various air mass fluxes is estimated based on the bulk density of the fuel samples in the reactor bed by using the following relation.

$$\textit{Biomass consumption estimated}\ (g/h) = \textit{Bed movement}\ (m/h) \times \textit{reactor area}\ (m^2) \times \textit{bulk density}\ (g/m^3).$$

It is observed that in the case of flaming combustion, particle sphere diameter decreases by about 10% and weight losses by 75–80% [25]. As the flame front temperature exceeds about 773 K, pyrolysis process is assumed to be complete leaving behind the char. Fuel consumption is estimated based on the bed movement at an air mass flux, and no char is removed during the experiment. The fuel sample size considered during the experiment is 14 × 10 × 10 mm with a bulk density of 370 kg/m^3 and the reactor diameter is 103 mm. It is also clear from the temperature profile and the data reported in the literature that the flame front is about 1.8 to about 3 particle depths depending upon the mass flux [12]. In the present study, the reaction zone thickness where the flame front exists is between 20 to 30 mm. Thus, below the propagation front in the packed bed, is mostly char, a product of pyrolysis. It

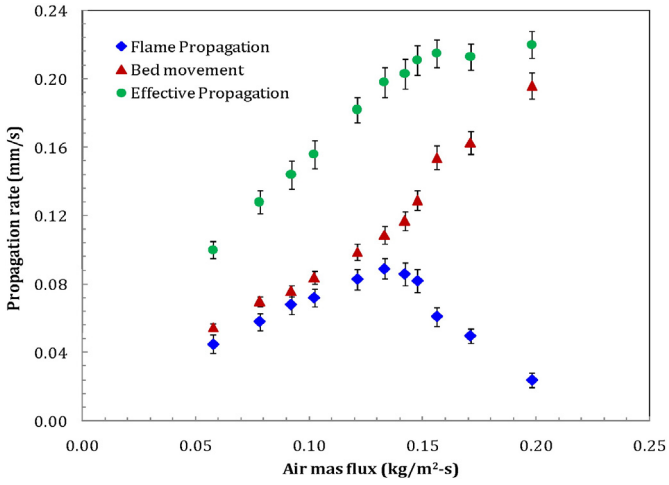

Fig. 9. Flame propagation, bed movement and effective propagation at different air mass flux.

can be concluded from this analysis that in the co-current reactor, the flame propagation rate movement is also an important parameter compared to effective propagation which helps to decide the operating range of a gasification system. It is also observed that with the increase in air mass flux, the char consumption rate increases below the pyrolysis zone. Any further increases in air mass flux enhance the char consumption, and it is depleted when it crosses the extinction limit and leads to non-performing conditions of the gasification system. There is a fair agreement with the data from these two independent methods considering less than 10% char is left over after the gasification process. This fair assumption is based on extensive experiments implying that total carbon conversion is not achieved during the gasification process [24].

4.3. Comparison of the results with literature reported data

Fig. 10 presents the peak bed temperatures measured during the experiment in two different capacity/size gasifier, model estimation of the peak bed temperature and the reported data from the literature. It is observed that as the air mass flux increases, peak bed temperature also increases and it is important to note that the situation in the reactor is always in fuel-rich conditions for the gasification process. It can be concluded from Fig. 10 that peak temperature estimation through the model follows a similar trend of the experimental measurements. Considering that the difference in density, shape and size of the particles influences the bed porosity, the differences in the peak temperatures in case of Fatehi and Kaviany, Rönnbäck et al. and experimental results of 35 kg/h gasifier rated capacity is justified [12,15]. Fathehi and Kaviany used fuel sample of spherical diameter of 6.4 mm and Rönnbäck et al. used pine wood with a diameter of 8 mm in reverse downdraft configurations [12,15]. Rönnbäck et al. found that the ignition rate and ignition front temperature (bed temperature) are strongly dependent on the air flow rate [15]. Horttanainen et al. found that the optimal air flow rate at which the propagation rate is maximum is lower for the fuels which constitute small particles and maximum propagation rates are achieved at fuel rich conditions [12]. Yang et al. reported that the reaction zone thickness in the bed increases as the combustion proceeds and becomes very hot before the combustion ends [26]. The data from Fathehi and Kaviany is used in the fuel rich (gasification) regime [12]. This study also observed that the burning rate increases as the air flow rate increases until a peak point is reached, beyond which further increase in the air flow rate reduces the burning rate. Porteiro et al. experimental study in the counter-current process observed that air mass flow rate

Table 4
Flame front, bed movement, effective propagation movement and biomass consumption at different air mass flux.

Air mass flux (kg/m^2-s)	Flame front movement (mm/s)	Bed movement (mm/s)	Effective propagation movement (mm/s)	Biomass consumption (g/h)		Difference in biomass consumption (%)
				experiment	estimation	
0.057	0.0454	0.0550	0.1004	551.6	610.1	9.6
0.086	0.0546	0.0680	0.1226	681.2	754.3	9.7
0.106	0.0696	0.0850	0.1546	873.8	942.9	7.3
0.121	0.0825	0.1000	0.1825	999.0	1109.3	9.9
0.134	0.0890	0.1090	0.1980	1111.8	1209.1	8.0
0.142	0.0867	0.1160	0.2027	1164.1	1286.8	9.5
0.147	0.0823	0.1280	0.2103	1261.9	1419.9	11.1
0.171	0.0507	0.1620	0.2127	1589.3	1797.1	11.6

is one of the parameters that has the most influence on ignition front propagation velocity [16]. It is also found that the maximum front velocity is achieved at sub-stoichiometric conditions, as the cooling effect due to excess air is minimum.

Fig. 11 represents the effective movement at different air mass flux. In downdraft or co-current configurations, fuel and air move downwards. Bed movement is the result of particle size reduction during the pyrolysis and further char consumption in the bed. The bed movement (downwards) depends on the overall biomass consumption. In the present study, the effective propagation rate or movement is a parameter identified as the sum of bed movement (downwards) and propagation rate (upwards) along with the results from literature [13–15]. It can be observed that the effective propagation rate increases with the increase in air mass flux. As the air mass flux increases, reactant fraction increases in the bed, i.e. enhanced the oxidising environment in the bed leads to higher fuel consumption. The higher fuel consumption leads to increase in bed movement and consequently a net increase in effective propagation rate. However, beyond a certain mass flux, the effective propagation rate profile nearly stagnates. This must be contrasted with the flame propagation rate profile (Fig. 6) where it reaches a maximum at a particular air mass flux and beyond this point, flame propagation movement rate starts decreasing. However, when the rate of increase in bed movement due to fuel consumption and shrinkage is dominated the flame propagation rate decreases beyond the critical mass flux. In the case of model estimation, it is observed that the effective movement linearly increases with the increase in air mass flux. The model estimation has a good agreement at lower air mass flux but differs at the higher air mass flux regimes.

Fig. 11 also presents the effective propagation rate reported by Gort, Horttaninen et al., Rönnbäck et al., Porteiro et al. [13–16]. It can be observed that except Horttaninen et al. (wood chips), Porteiro et al. (pine shavings) results, all other results falls under a narrow band and follows the pattern with the model estimation [14,16]. The surface area/volume ratio for wood chips and pine shavings is relatively higher than all other cases (Table 1). Similarly, the bulk density is also lower in these two fuel samples than the other fuels considered in Fig. 11 and hence the void fraction is also high (Table 1). Horttaninen et al. observed that the increase in bed porosity makes the flame propagation quicker since the thermal energy required to heat the bed reduces and also inter-particle heat transfer enhanced due to the higher surface area/volume ratio [14]. Thus, the higher surface area/volume and lower bulk density are the reasons for higher propagation rate for wood chips and pine shavings. Gort and Horttaninen et al. also showed that particle size does not have any significant effect on the propagation rate [13,14]. The difference in the propagation rate is strongly dependent on the physical properties of fuel (surface area/volume ratio) apart from other properties like fuel conversion and possible heat loss from the reactor wall also influences the temperature profile in the packed bed.

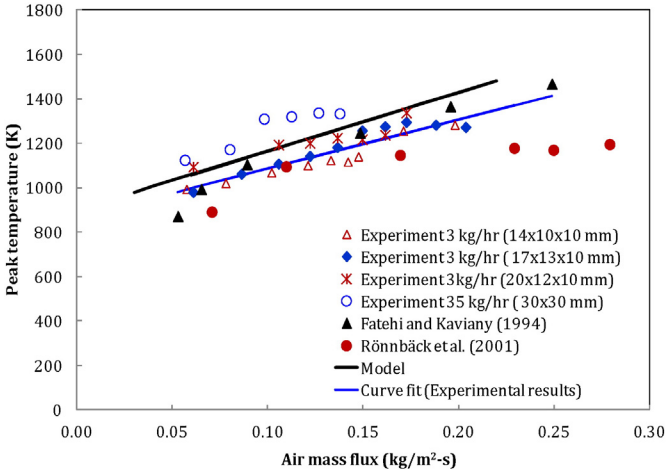

Fig. 10. Peak bed temperatures at various air mass flux.

Fig. 12 presents the results of effective propagation rate normalized with bulk density to address the observed variations of Fig. 11. Fig. 12 also represents the air mass flux, at which flame propagation achieves negative value. It can be observed from Fig. 12 that at the extinction point, the flame propagation profile changes its direction. The physical significance of extinction is the upward flame propagation rate is zero, rather flame moves downward in the char bed. This situation happens at higher air mass flux or the gasification regimes slowly changes towards combustion regimes. As all the experiments are carried out in the sub-stoichiometric regimes, the experimental measurements of this study limited up to the extinction point. There is no measurement beyond the extinction points. However, in the reported literature, in reverse downdraft configurations, where combustion processes are characterized, there are measurements beyond this extinction limit [12,13,15]. The overall trend of the model estimation closely lies in a narrow band of all the experimental measurements and the literature data up to the extinction limit line.

4.4. Prediction of exit gas composition at different air mass flux

The volume fraction of various gaseous species which evolved at the reactor exits for different reactant mass flux is presented in Table 5 and compared with the experimental measurements. The gaseous species comprises of CO, CO_2, H_2, CH_4, N_2 and H_2O. The hot moist output gas is used to arrive at the dry gas mole fraction used in the present analysis to compare with the experimental results. It can be observed from the model estimation that the CO fraction is maximum (18.78%) at an air mass flux of 0.115 $kg/m^2/s$. Both the model estimation and experimental measurement shows that the variations of CO fraction over the range of air mass flux are very low. It is also observed from Fig. 5 that the peak propagation front rate occurs at 0.135 $kg/m^2/s$ for model estimation and

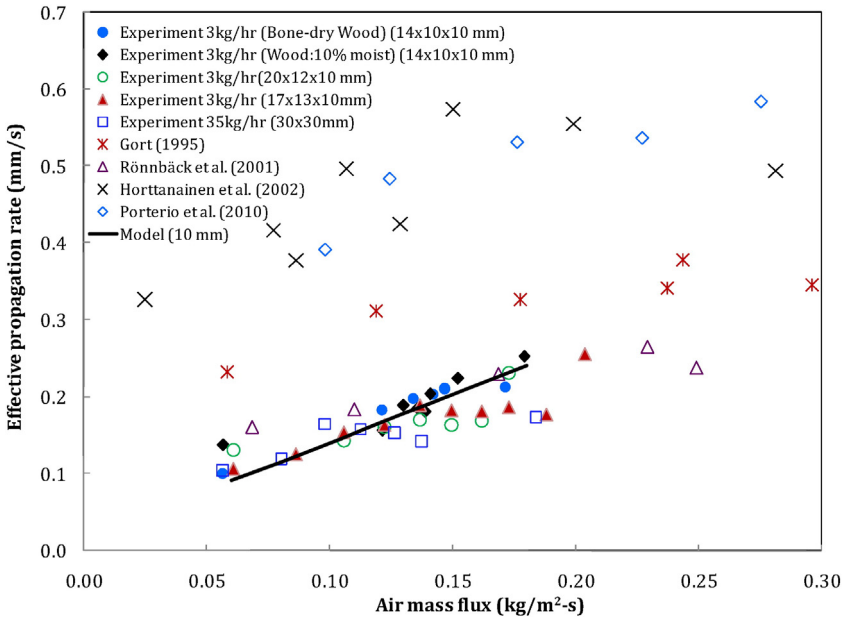

Fig. 11. Effective movement from model and experiment at various air mass fluxes.

0.132 kg/m^2/s for experimental measurements. Hence, it can be concluded that CO fraction is almost constant in a close band of peak propagation front regimes. This also concludes that, if the gasifier operates at an air mass flux close to the peak propagation front, CO fraction will be nearly the same in this operation range. It is also important to note that with the increase in bed temperature, CO_2 concentration increases. However, as the operation range in the gasification regime kept in this air mass flux regimes, the increase in CO_2 concentration is not significant. The maximum H_2 fraction in the model estimation is 16.18% at an air mass flux of 0.14 kg/m^2/s and in the case of experimental measurement; it is 13.85% at an air mass flux of 0.142 kg/m^2/s. It can be observed that as the air mass increases, H_2 fraction increases and reaches a maximum point and then decreases. The analysis related to the gas composition, model estimation and experimental measurement shows that the gas composition is nearly constant in the entire air mass flux range. This suggests that the overall reaction occurs in substoichiometric regimes in the bed. It is also found from the equilibrium analysis that this type of gas composition occurs at air to fuel ratio in the range of 1.5–1.8, which is the typical condition for the gasification process. Considering the variations in various properties (particle sizes, thermo-physical properties), operating parameters (different mass flux) the predicted gas composition results are assumed to have good agreement with the experimental measurements.

4.5. Influence of surface area of particle on gasification process

Numerical analysis and experiments are carried out to address the influence of particle surface area on the overall process, for the varying surface area per unit volume (SA/V) ratio in the packed bed reactor. As the surface area per unit volume of the reactor increases, the higher

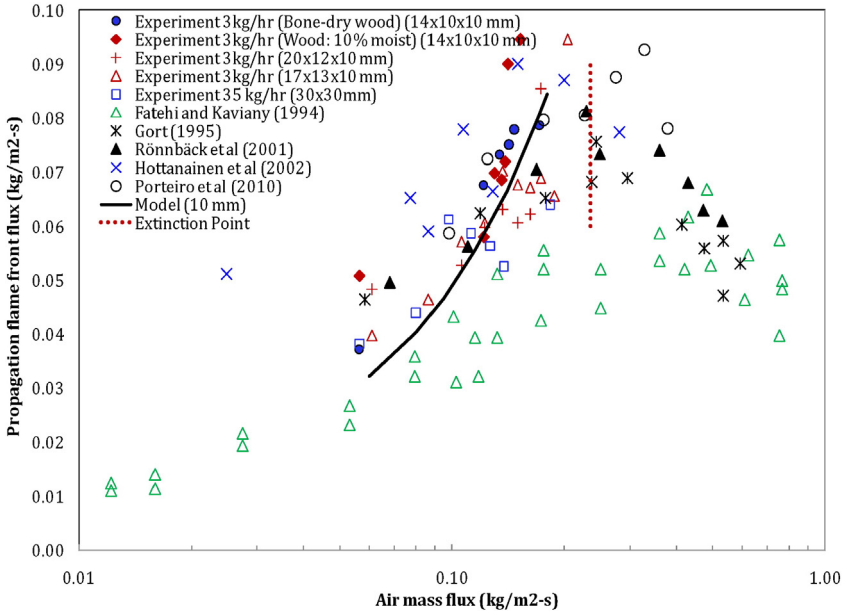

Fig. 12. Propagation flame front flux from model and experiment at various air mass fluxes.

Table 5
Volume fraction of different gases from model and experiment at various air mass fluxes.

Model				Experiment			
Air mass flux (kg/m^2-s)	CO_2 (%)	CO (%)	H_2 (%)	Air mass flux (kg/m^2-s)	CO_2 (%)	CO (%)	H_2 (%)
0.060	17.98	17.25	13.02	0.058	15.00	16.09	8.65
0.080	16.85	17.98	13.76	0.078	15.05	15.84	9.52
0.095	16.46	18.56	14.54	0.102	14.90	15.15	10.85
0.105	16.23	18.69	14.98	0.121	14.95	15.29	11.15
0.115	16.26	18.78	15.54	0.133	15.11	15.92	12.97
0.130	16.42	18.62	16.14	0.142	14.89	15.34	13.85
0.140	16.77	18.32	16.18	0.148	13.10	16.09	12.86
0.160	17.25	17.72	15.92	0.171	14.33	16.27	8.89
Average	16.78 ± 0.59	18.24 ± 0.54	15.01 ± 1.16	Average	14.89 ± 0.28	15.75 ± 0.43	11.09 ± 1.99

molecular weight fraction products of pyrolysis, identified as a volatile fraction is considered as a species from the reactor output. Mahapatra and Dasappa have addressed the influence of particle size on the gasification from experimental measurements and clearly identified that at higher SA/V ratio, tar levels is high [27]. An attempt is made here to address this aspect using the model results. Fig. 13 presents the conversion time variation and the unreacted volatile fraction with surface area/volume ratio of the particle. Data set for air mass flux is fixed at 0.105 kg/m^2/s, with varying particle size, with no moisture in the fuel is presented in Fig. 13. It is observed from Fig. 13 that as the SA/V increases, the conversion time reduces, means smaller the particle (larger SA/V), conversion time is lower in compare with larger particle size (lower SA/V). Babu and Chaurasia also observed that the spherical particle has lesser conversion time compared to the slab shape particle, due to higher surface/volume ratio [28]. It is also known from the literature that the d^2 law prevails during the major part of the biomass combustion [25]. It is found from Fig. 13 that the conversion time varies with $(SA/V)^{-1.54}$. The time for pyrolysis is inversely proportional to the surface area, thus increase in the surface area leads to increase in the pyrolysis rate at the same temperature [29]. It is also important to mention that the pyrolysis of the smaller particle is mainly controlled by reaction kinetics, whereas for the larger particle, process is mainly controlled by diffusion. Further, larger particle has higher heat transfer resistance and hence, the actual temperature inside the particle is lower, leading to products of slow pyrolysis. However, in the case of smaller particles, it could transit to fast pyrolysis depending upon the temperature with products having larger fractions of volatiles. Simmons and Ragland reported that with the reduction of particle size, burning rate per unit mass increases linearly [30]. Mason et al. observed as the aspect ratio

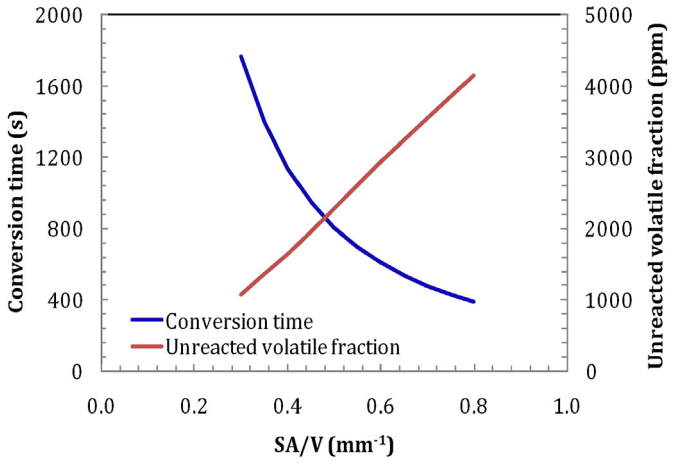

Fig. 13. SA/V vs conversion time and unreacted volatile fraction.

increase; volatile burn time becomes quicker [31]. The model estimation results analysis has a good agreement with the findings of the literature.

5. Conclusions

The packed bed model for co-current downdraft gasification system is used to estimate the propagation rate, effective propagation rate, bed temperature, gas composition, and unreacted volatile fractions in the bed. The model predictions compare well with the present experimental results, and also those found in the literature with respect to counter and co-current reactor configuration on the flame propagation and effective propagation rates. The peak propagation rate from the model is found to be 0.0941 mm/s at an air mass flux of 0.135 kg/m^2/s compared to the experimental results; it is 0.089 mm/s at an air mass flux of 0.132 kg/m^2/s. The general trend of propagation rate with air mass flux follows similarly in both the model and experiment. It is also found that beyond 0.225 kg/m^2/s air mass flux, flame front ceased and at an air mass flux of 0.235 kg/m^2/s, the front is receding, or moves towards the char bed, and this is justified due to balance between heat generation and heat loss in the reaction zone. Model estimation and experimental measurement suggest that as the air mass flux increases, peak bed temperature also increases. The effective propagation rate reported by various literature is also compared with the present experimental results and model estimation. Parametric variation of surface area per unit volume of the particles in the packed bed indicates that with the increase in SA/V ratio, conversion time reduces, and unreacted volatile fraction in the bed also increases. This study concludes that the surface area/volume is the critical parameter rather the particle size for estimation of conversion time or unreacted volatile fraction availability in the bed. This model analysis provides a comprehensive understanding with respect to the packed reactor under gasification conditions addressing the dependence on mass flux on gas composition and propagation rate with experimental validation of the results.

References

[1] T.K. Patra, P.N. Sheth, Biomass gasification models for downdraft gasifier: a state of the art review, Renew. Sust. Energ. Rev. 50 (2015) 583–593.
[2] D. Baruah, D.C. Baruah, Modeling of biomass gasification: a review, Renew. Sust. Energ. Rev. 39 (2014) 806–815.
[3] A. Melgar, J.F. Perez, H. Laget, A. Horillo, Thermo-chemical equilibrium modeling of a gasifying process, Energy Convers. Manag. 48 (1) (2007) 59–67.
[4] A.H. Mahmoudi, M. Markovic, B. Peters, G. Brem, An experimental and numerical study of wood combustion in a fixed bed using Euler–Lagrange approach (XDEM), Fuel 150 (2015) 573–582.
[5] S. Dasappa, P.J. Paul, H.S. Mukunda, U. Shrinivasa, Wood-char gasification: experiments and analysis on single particles and packed beds, Symp. Combust. 27 (1) (1998) 1335–1342.
[6] A.H. Mahmoudi, F. Hoffmann, B. Peters, Detailed numerical modeling of pyrolysis in a heterogeneous packed bed using XDEM, J. Anal. Appl. Pyrolysis 106 (2014) 9–20.
[7] K. Sandeep, S. Dasappa, Packed bed model for biomass gasification, CGPL Technical Report, Indian Institute of Science, Bangalore, 2015.
[8] E. Ranzi, M. Corbetta, F. Manenti, S. Pierucci, Kinetic modeling of the thermal degradation and combustion of biomass, Chem. Eng. Sci. 110 (2014) 2–12.
[9] C. Di Blasi, Modeling wood gasification in a countercurrent fixed-bed reactor, AICHE J. 50 (9) (2004) 2306–2319.
[10] S. Mahapatra, S. Dasappa, Experiments and analysis of propagation front under gasification regimes in a packed bed, Fuel Process. Technol. 121 (2014) 83–90.
[11] S. Dasappa, P.J. Paul, Gasification of char particles in packed beds: analysis and results, Int. J. Energy Res. 25 (12) (2001) 1053–1072.
[12] M. Fatehi, M. Kaviany, Adiabatic reverse combustion in a packed bed, Combust. Flame 99 (1) (1994) 1–17.
[13] R. Gort, On the propagation of a reaction front in a packed bed, thermal conversion of municipal solid waste and biomassPhD Thesis University of Twente, 1995.
[14] M. Horttanainen, J. Saastamoinen, P. Sarkomaa, Operational limits of ignition front propagation against airflow in packed beds of different wood fuels, Energy Fuel 16 (3) (2002) 676–686.
[15] M. Rönnbäck, M. Axell, L. Gustavsson, H. Thunman, B. Leckner, Combustion processes in a biomass fuel bed — experimental results, Progress in Thermochemical Biomass Conversion 2001, pp. 743–757.
[16] J. Porteiro, D. Patino, J. Collazo, E. Granada, J. Moran, J.L. Miguez, Experimental analysis of the ignition front propagation of several biomass fuels in a fixed-bed combustor, Fuel 89 (1) (2010) 26–35.

[17] J. Ohlemiller T., J. Bellan, Rogers F., A model of smoldering combustion applied to flexible polyurethane foams, Combust. Flame 36 (1) (1979) 197–215.
[18] S. Dasappa, Experimental and modeling studies on the gasification of wood-charPhD Thesis Indian Institute of Science, India, 1999.
[19] M.J. Groeneveld, The co-current moving bed gasifierPhD Thesis Twente University of Technology, Netherlands, 1980.
[20] J. Goldman, D. Xieu, A. Oko, R. Milne, R.H. Essenhigh, A comparison of prediction and experiment in the gasification of anthracite in air and oxygen-enriched steam mixtures, Symp. Combust. 20 (1) (1985) 1365–1372.
[21] J.B. Howard, Combustion of carbon with oxygen, MIT Technical Report, 1967.
[22] J.D. Blackwood, F. McGrory, The carbon steam reaction at high pressure, Aust. J. Chem. 11 (1) (1958) 16–23.
[23] SERI, Generator Gas — The Swedish Experience From 1938 to 1945 (Translation), Solar Energy Research Institute, Colorado, 1979 (NTIS/S 33-140).
[24] H.S. Mukunda, P.J. Paul, S. Dasappa, U. Shrinivasa, H. Sharan, R. Buehler, P. Hasler, H. Kaufmann, Results of an Indo-Swiss programme for qualification and testing of a 300-kW IISc-Dasag gasifier, Energy Sustain. Dev. 1 (4) (1994) 46–49.
[25] H.S. Mukunda, P.J. Paul, U. Shrinivasa, N.K.S. Rajan, Combustion of wooden spheres — experiments and model analysis, Symp. Combust. 1619-1628 (1984).
[26] Y.B. Yang, V.N. Sharifi, J. Swithenbank, Effect of air flow rate and fuel moisture on the burning behaviours of biomass and simulated municipal solid wastes in packed beds, Fuel 83 (11–12) (2004) 1553–1562.
[27] S. Mahapatra, S. Dasappa, Influence of surface area to volume ratio of fuel particles on gasification process in a fixed bed, Energy Sustain. Dev. 19 (2014) 122–129.
[28] B.V. Babu, A.S. Chaurasia, Heat transfer and kinetics in the pyrolysis of shrinking biomass particle, Chem. Eng. Sci. 59 (10) (2004) 1999–2012.
[29] T. Phuphuakrat, N. Nipattummakul, T. Namioka, S. Kerdsuwan, K. Yoshikawa, Characterization of tar content in the syngas produced in a downdraft type fixed bed gasification system from dried sewage sludge, Fuel 89 (9) (2010) 2278–2284.
[30] W.W. Simmons, K.W. Ragland, Burning rate of millimeter sized wood particles in a furnace, Combust. Sci. Technol. 46 (1) (1986) 1–15.
[31] P.E. Mason, L.I. Darvell, J.M. Jones, M. Pourkashanian, A. Williams, Single particle flame-combustion studies on solid biomass fuels, Fuel 151 (2015) 21–30.